Microporous and Mesoporous Materials 185 (2014) 235–244

Contents lists available at ScienceDirect

Microporous and Mesoporous Materials

journal homepage: www.elsevier.com/locate/micromeso

# Thermophysical properties of MOF-5 powders

Yang Ming [a], Justin Purewal [b], Dong'an Liu [b], Andrea Sudik [c], Chunchuan Xu [c], Jun Yang [c], Mike Veenstra [c], Kevin Rhodes [c], Richard Soltis [c], James Warner [c], Manuela Gaab [d], Ulrich Müller [d], Donald J. Siegel [b,*]

[a] Department of Physics, University of Michigan, 1440 Randall Laboratory, 450 Church St., Ann Arbor, MI 48109-1040, USA
[b] Mechanical Engineering Department, University of Michigan, 2250 G.G. Brown Laboratory, 2350 Hayward St., Ann Arbor, MI 48109-2125, USA
[c] Ford Motor Company, Research and Advanced Engineering, MD 1170/RIC, P.O. Box 2053, Dearborn, MI 48121, USA
[d] BASF SE, Process Research and Chemical Engineering, 67056 Ludwigshafen, Germany

ARTICLE INFO

*Article history:*
Received 12 August 2013
Received in revised form 4 November 2013
Accepted 8 November 2013
Available online 19 November 2013

*Keywords:*
Metal organic frameworks
Thermophysical properties
Gas capture and storage
Hydrogen storage

ABSTRACT

We present a comprehensive assessment of the thermophysical properties of an industrial, pilot-scale version of the prototype adsorbent, metal–organic framework 5 (MOF-5). These properties are essential ingredients in the design and modeling of MOF-5-based hydrogen adsorption systems, and may serve as a useful starting point for the development of other MOF-based systems for applications in catalysis, gas separations, and adsorption of other gasses or fluids. Characterized properties include: packing density, surface area, pore volume, particle size distribution, thermal conductivity, heat capacity, stability against hydrolysis, differential enthalpy of $H_2$ adsorption, and Dubinin–Astakhov isotherm parameters. Hydrogen adsorption/desorption isotherms were measured at six temperatures spanning the range 77–295 K, and at pressures of 0–100 bar.



## 1. Introduction

Metal–organic frameworks, a relatively new class of crystalline, high-surface area materials [1,2], are in the process of transitioning from the laboratory to commercial applications [3–9]. To facilitate this transition, knowledge of the physical and thermal properties of MOFs, typically in powder form, is essential. This data is needed for applications including gas capture and storage, catalysis, and gas separations.

In the case of hydrogen storage, we note that an abundance of $H_2$ uptake measurements exist for MOFs [2,10,11]. Nevertheless, several other material properties needed for the design and modeling of a complete hydrogen storage system have received much less attention. For example, models originally developed for packed bed adsorbents used in pressure swing adsorption (PSA) processes have been adapted for sorption-based hydrogen storage at cryogenic [12] and ambient conditions [13]. These models aim to describe thermal and mass-transfer effects during charge and discharge. However, when parameters in the governing equations are not known from measurements, they must be estimated from existing, and potentially incompatible data. The availability of accurate thermophysical properties such as packing density, thermal conductivity, particle size distribution, along with an accurate equilibrium pressure–temperature-composition (PCT) equation of state for the adsorbed hydrogen, will greatly benefit the accuracy of these models and allow their use in making performance projections and for design optimization.

It is well known that differences in synthesis, filtration, drying, activation, and shaping can result in a wide variation in MOF properties such as pore volume, surface area, and crystallite size [14–17]. However, with the advent of reproducible, commercial-scale production techniques [18,19], it is now possible to establish a "standard" set of properties for many MOFs. Here we present measurements of structural, thermal, and hydrogen storage properties of the benchmark cryo-adsorption material MOF-5. While many of MOFs have been reported, here we focus on MOF-5 as it represents the most widely studied MOF [20]. MOF-5 consists of $ZnO_4$ clusters connected by 1,4-benzenedicarboxylate (BDC) linkers. We report an extensive set of MOF-5 material properties, including: density (and its dependence on tapping conditions), surface area, pore volume, particle size distribution, thermal conductivity, heat capacity, robustness with respect to humid air, and differential adsorption enthalpy. We also determine parameters for a modified Dubinin–Astakhov [21] model in order to predict the uptake of adsorbed $H_2$ within MOF-5 over the temperature range of 77–295 K and the pressure range of 0–100 bar. The MOF-5 properties reported here should facilitate predictions of system-level properties such as hydrogen discharge pressures, refueling dynamics, and capacity, while enabling other MOF applications beyond hydrogen storage.

## 2. Experimental procedure

### 2.1. Materials preparation

A summary of the conventional and electrochemical-based processes for industrial MOF synthesis is given in Ref. [4]. The conven-

* Corresponding author. Tel.: +1 734 764 4808.
*E-mail address:* djsiege@umich.edu (D.J. Siegel).

1387-1811/$ - see front matter © 2013 Elsevier Inc. All rights reserved.
http://dx.doi.org/10.1016/j.micromeso.2013.11.015

tional synthesis process for MOFs involves combining metal salts (e.g., metal nitrates, sulfates, or acetates) with multi-topic organic linkers, the latter most commonly consisting of mono-, di-, tri- or tetracarboxylic acids. These constituents are dissolved together and stirred in a polar organic solvent such as an amine [e.g. triethylamine (TEA)] or amide [e.g. *N*,*N*-diethylformamide (DEF), *N*,*N*-dimethylformamide (DMF)]. MOF crystallites then form via self-assembly and subsequently precipitate from the solution within minutes to hours. Typical synthesis temperatures range from ambient up to approximately 200 °C. After filtration, washing, and drying, the crystalline product is obtained in the form of a powder. Depending on the desired application, the powder can be further processed into compacts (e.g., pellets, strands, etc.) [4,22,23].

Laboratory-scale MOF synthesis procedures have recently been scaled from multi-kg to tons of product per batch, which will facilitate commercial applications of these materials [18,19]. Moreover, sustainability is a big concern and was achieved by replacing solvent-based by water-based procedures [19]. Example space–time-yields (STY) for the synthesis of MOF (and other framework) materials observed in laboratory and industrial settings are given in Table 1. Up to three orders of magnitude improvement in STY is observed in transitioning from laboratory to commercial settings.

In the present study, MOF-5 powders were synthesized by BASF at room temperature using a procedure described by Yaghi and coworkers starting from 1,4-benzene dicarboxylic acid ($H_2BDC$, $C_8H_6O_4$, Merck), zinc acetate dihydrate ($Zn(CH_3COO)_2{\cdot}2H_2O$, Merck), and *N*,*N*-dimethylformamide (DMF, BASF AG) [24]. In a glass reactor equipped with a Teflon-lined stirrer, 130 g of $Zn(CH_3COO)_2{\cdot}2H_2O$ was dissolved in 1200 mL DMF. Within 2 h, a solution of 37.5 g of $H_2BDC$ in 950 mL DMF was added under rigorous stirring. The precipitate was filtered off, washed three times with 1 L of dry acetone and dried under a stream of flowing nitrogen. Given the low vapor pressure of conventional MOF synthesis solvents (e.g. DMF has a vapor pressure of approximately 4 torr at 25 °C), solvent exchange to a more volatile solvent (e.g. acetone has a vapor pressure of approximately 270 torr at 25 °C) has been shown to be an effective method for solvent removal. Prior to characterization, MOF-5 was heated and evacuated at 130 °C and 50 mtorr for 1–3 h, yielding the desolvated or so-called 'activated' form of the material. An alternative route to desolvation of MOFs involves a liquid or super-critical $CO_2$ solvent removal process [25]. The wet chemical analysis of the obtained solid yielded 34 wt.% Zn, equivalent to 92% molar yield of MOF-5 calculated as $Zn_4O(BDC)_3$. The concentration from residual nitrate amounted to be less than 0.05 wt.% N. Cubic shaped crystals with a size of <1 μm were observed by scanning electron microscopy (see Section 3.1.3 below). Powder X-ray diffraction was also performed to characterize the crystallites. (See Fig. 12 in Section 3.4.)

## 2.2. Materials characterization

An extensive set of techniques was used to characterize several properties of the MOF-5 powders obtained, including: crystallinity, surface area, pore volume, particle size distribution, density, heat capacity, thermal conductivity, robustness with respect to humidity, and hydrogen storage properties.

### 2.2.1. Powder X-ray diffraction (PXRD)

MOF-5 powders were loaded into a flat sample holder under a dry nitrogen atmosphere and covered with a plastic foil to minimize degradation due to air moisture during analysis. The samples were measured at room temperature in reflection mode with a powder X-ray diffractometer (Rigaku Miniflex II, Cu Kα, λ = 1.5418 Å) between 2° and 70° (2-Theta) with a step width of 0.02° and a measurement time of 3.6 s per step. The powder X-ray diffraction (XRD) pattern was obtained using a scanning rate of 0.33°/min with $2\theta$ from 2° to 70°.

### 2.2.2. Surface area and pore volume

Surface area was measured at 77 K using nitrogen sorption in an Autosorb AS6B-KR (Quantachrome Instruments). Prior to the measurement, the MOF-5 sample (31.6 mg) was placed in the sample cell and activated at $10^{-4}$ mbar for 2 h at 130 °C. Surface area values were calculated using the Brunauer–Emmet–Teller (BET) equation [26] according to DIN 66131 (Determination of specific surface area of solids by means of gas adsorption after BET). The pore volume and area distribution were calculated applying the Barrett–Joyner–Halenda (BJH) equation [27] on the isotherm data according to DIN 66134 (Mesopore Analysis by Nitrogen Sorption using the Method of BJH). (See Section 3.1.1 below for results)

### 2.2.3. Particle size

Scanning electron microscopy (SEM) images were taken with a JEOL JSM 6400F Field Emission SEM with an acceleration voltage of 5 kV. Prior to SEM imaging, the MOF crystals were sputtered with a thin Au/Pd layer to make their surface electrically conducting. ImageJ software was used for image analysis [28]. Crystal size statistics were determined based on three unique SEM images comprising a total of 182 measured MOF-5 crystallites. The crystals generally possessed a cubic morphology; diameter measurements were taken along the diagonal of the cube face. (See Section 3.1.2 below for results.)

### 2.2.4. Density

The volumetric density of stored hydrogen is an important performance metric for mobile fuel cell applications. The densities of high-surface-area materials can be quite low, ranging from 0.1 to 0.4 g/cm$^3$ [22,23]. Consequently densification into pellets or custom-molded monoliths has been explored for such materials as MOF-177 [29,30], MOF-5 [23] and activated carbons [31], resulting in higher densities of 0.5–0.8 g/cm$^3$.

Three varieties of density are of relevance for MOF powders: bulk density, framework density, and single crystal density. Bulk powder density includes all interparticle voids, along with all open and closed pore intraparticle volumes, as part of the total sample volume. In contrast, the framework density (i.e., skeletal density) includes only closed pore volumes and the volume occupied by the covalently-bonded framework atoms. Single crystal density includes both open and closed pore volumes.

**Table 1**
Comparison of space–time-yields (STY) for synthesis of various framework materials in both laboratory and commercial settings.

| Composition | Literature name | Laboratory STY (kg/m$^3$/d) | Ref. | Commercial name | Industry STY (kg/m$^3$/d) | Ref. |
|---|---|---|---|---|---|---|
| $Zn_4O(BDC)_3$ | MOF-5 IRMOF-1 | 0.21 | [72] | Basolite Z100H | 299 | – |
| $Cu_3(BTC)_2$ | HKUST-1 | 8.6 | [72] | Basolite C300 | 225 | [4] |
| $Zn(MeIM)_2$ | ZIF-8 | 1.3 | [72] | Basolite Z1200 | 160 | [4] |
| Aluminum–fumarate | Aluminum–fumarate MOF | ~30 | [72] | Basolite A520 | up to >3600 | [19] |

MeIM = 2-Methylimidazolate, BTC = benzene-1,3,5-tricarboxylate, BDC = 1,4-benzene dicarboxylate.

Measurements of bulk density can result in a range of values due to differences in the number of taps (if any), size of the container, packing force, and particle size (the latter quantity can itself be affected by the processing procedure, e.g., milling). In gas storage applications it is desirable to completely fill the storage vessel with MOF powder in a manner that minimizes the presence of large voids. Repeated tapping and/or vibration of the powder and vessel can accomplish this. A standardized value for the packing or tap density can be measured using DIN ISO 787 Part II, ISO 3953, or ASTM B 527-93 using a jolting volumeter. The bulk density ($\rho_{bulk}$) of MOF-5 was determined by completely filling a stainless steel cylindrical vessel of known mass and volume (0.75 mL) with MOF powder. The filling process involved the incremental addition of small amounts of material to the vessel followed by light tapping. Measurements were repeated three times; the measured values deviate from one another by less than 5%. Additional measurements were performed using different numbers of taps and container volumes to evaluate the effects on tap density. In addition, a tap density measurement was taken using the standardized jolting volumeter.

The single crystal density ($\rho_{sx}$ = 0.605 g/cm$^3$) was obtained from Ref. [16]. The framework density ($\rho_{fm}$), or skeletal density, was determined by helium density measurements using an AccuPyc 1330 Pycnometer (Micrometritics). For this measurement 8.0 mL of MOF-5 was placed in the standard sample holder at ambient temperature. Research grade helium was used. The measurements were repeated until the reproducibility was within ±0.005 g/mL.

*2.2.5. Heat capacity*

The heat capacity ($c_p$) was measured by a dynamic heat flow difference calorimeter (Mettler TA 3000). The MOF-5 sample (5.5 mg) was placed in an open alumina crucible under inert nitrogen and heated at a rate of 5 °C/min from approximately 220–370 K with a metering range of 10 mW. The difference in the amount of heat required to increase the temperature of the sample compared to that of the reference material (sapphire with $c_p$ = 30.9 mg) is measured as a function of oven temperature according to DIN 51007 (general principles of differential thermal analysis).

*2.2.6. Thermal conductivity*

The thermal conductivity of MOF-5 was calculated based on the product of its heat capacity, thermal diffusivity, and density. Thermal diffusivity measurements were performed with a commercial xenon flash thermal diffusivity instrument (Anter Flashline, FL3000S2) operating at 700 W, using 12.7 mm diameter pellets with an average thickness of 2 mm and densities of 0.35, 0.52, and 0.69 g/cm$^3$. The pellets were kept under a $N_2$ atmosphere during measurements to limit the effects of humidity. A thin layer of silver paint was applied to the top surfaces of the pellets to prevent them from fracturing during measurement. The lower surfaces (i.e., the side incident to the light) of the pellets were coated with graphite to improve adsorption of light. A 5 K/min ramp rate was used [32].

*2.2.7. Hydrogen storage isotherms*

Hydrogen adsorption measurements were performed using an automated Sievert's-type apparatus (Setaram, PCT-Pro 2000) with an oil-free scroll vacuum pump (Anest Iwata, model ISP90). The mass of MOF-5 loaded for adsorption measurements was 436 mg. Prior to measurements, the MOF-5 powder was activated for at least 6 h under continuous vacuum (3 h at room temperature followed by 3 h at 130 °C). The void volume of the sample, vessel, and gas lines was determined based on the expansion of low-pressure (<5 bar) helium gas while maintaining isothermal conditions at approximately 28 °C. This assumes that helium does not appreciably interact (adsorb) with the MOF sample under these conditions.

Adsorption isotherms were measured at six sample temperatures: 77, 103, 118, 138, 200 and 295 K. The 77 K isotherm was measured by immersing the sample holder in a liquid nitrogen bath; the 200 K isotherm was measured by covering the sample holder in solid $CO_2$ powder; the 295 K isotherm was measured at ambient temperature. For intermediate temperatures (103 K, 118 K, 138 K), the sample was cooled to the target temperature using a continuous flow liquid nitrogen cryostat (CryoPro-2009, Setaram). The sample temperature was monitored with an internal platinum resistance thermometer in direct contact with the powder. The temperature of the sample vessel was regulated by a temperature controller that operates heaters located on the exterior of the sample vessel and bottom of the Dewar surrounding the sample vessel. The sample vessel was allowed to equilibrate at the target temperature for approximately 1 h.

Hydrogen adsorption isotherms were measured by the volumetric method [33]. To correct errors caused by the temperature gradient between the reservoir sub-volume (maintained at 27.6 °C), sample sub-volume (set at cryogenic target temperature), and tubing sub-volume ($^1/_8''$ tubing to minimize the volume), a separate hydrogen density was calculated for each sub-volume. A calibration test was performed using non-porous $Al_2O_3$ powder for each sample temperature, using conditions (e.g. reservoir and sample volumes, etc.) identical to that for the sample. Maximum error during calibration tests was typically 0.3 mmol of $H_2$ (at 77 K), in comparison to the 10 mmol of $H_2$ that was adsorbed at 77 K. The equilibrium gas phase density ($\rho_g$) was calculated from the equation of state for normal hydrogen by Leachman et al. [34]. employed in the NIST Standard Reference Database [35]. All experiments used ultra-high purity grade (99.999%) hydrogen and helium.

*2.2.8. Robustness with respect to air exposure*

Previous studies have shown that MOF-5 will decompose in air under humid environments [36,37]. Consequently, robustness to humid air is an important property since it can impact the manufacturing and assembly of the material in a hydrogen storage system, as well as its long-term stability upon cycling. The impact of exposing MOF-5 to air was assessed using hydrogen uptake measurements (PCT-Pro 2000, Setaram) and time resolved X-ray diffraction. For PCT measurements, two grams of MOF-5 powders were removed from the glovebox and placed on the lab bench in contact with the ambient atmosphere for exposure times up to 8 h. For diffraction studies approximately 0.02–0.05 g were exposed for up to 250 h. As these experiments were meant to mimic an unintentional exposure event, the laboratory environment was not strictly controlled: exposure conditions were approximately 45% relative humidity and 22 °C. To assess whether changes to MOF-5 performance due to exposure were reversible by activation, PCT measurements were performed for samples with (activated) and without activation (non-activated), where the activation conditions are the same as previously described (minimum of 6 h total under continuous vacuum, with 3 h at room temperature followed by at least 3 h at 130 °C).

## 3. Results and discussion

Our discussion of MOF-5 properties is divided into three sections: structural properties, thermal properties, and hydrogen storage properties. These properties will strongly impact the design and performance of MOF-based hydrogen storage systems, and are essential input for the parameterization and validation of storage system models. A summary of the measured property data is given in Table 2.

### 3.1. Structural properties

We take the structural properties of an adsorbent to include its surface area, pore volume, density, and crystal size. These attributes strongly influence the gravimetric and volumetric densities of adsorbed species such as hydrogen. For example, the gravimetric excess hydrogen capacity of porous materials generally scales with surface area [38–40]. On the other hand, density, pore volume, and particle size control volumetric capacity. To some extent, bulk physical properties can be optimized through processing techniques. For example, compacting the material can increase density, and ensuring full removal of synthesis solvent from the MOF surfaces/pores can maximize surface area. Regarding compaction, a detailed study of the benefits associated with densification of MOF-5 powder into shaped bodies (tablets, strands, bars, etc.) [41] was previously reported by the authors [42]. Typically, a compromise exists between maximizing surface area and pore volume (or density) since materials with high surface area generally exhibit large pore volumes [43]. Thus, the gravimetric and volumetric capacities of an adsorbed species cannot be tuned independently. Lastly, we note that the crystalline pore structure of the MOF-5 powder obtained by the zinc acetate dihydrate synthesis [described in Section 2.1] is remarkably robust against both mechanical compaction [42] and degradation from moisture. (For XRD plots, see Section 3.4.)

#### 3.1.1. Surface area and pore volume

The specific surface area is a key factor that determines the hydrogen capacity of a given MOF. The amount of adsorbed hydrogen (often expressed as excess capacity), can be estimated by assuming monolayer hydrogen coverage on the sorbent surface with a density equal to that of liquid hydrogen [44]. Under this approximation, the excess hydrogen capacity per unit mass (i.e. excess gravimetric capacity) is proportional to the sorbent's specific surface area where the proportionality constant is: $2.28 \times 10^{-3}$ wt.% $H_2$ $m^{-2}$. That is, a MOF possessing a specific surface area ($SA$) of 500 $m^2$/g should store approximately 1 wt.% (excess) hydrogen (at 77 K) [40]. The agreement of this surface area versus excess uptake relationship has been demonstrated for a wide range of sorbents [45–47]. Differences in uptake for a given material have been observed largely stemming from differences in sorbent preparation and desolvation methods which lead to variation in surface area and hydrogen uptake measurements for a given material. For example, MOF-5 isolated and desolvated in air with conventional solvents has a BET surface area of ~3100 $m^2$/g (comparable to the value reported in this study), whereas identically prepared MOF-5 isolated and desolvated in a nitrogen atmosphere with anhydrous solvents has a BET surface area of 3800 $m^2$/g [48].

Significant effort has been devoted to improving excess gravimetric hydrogen capacity by increasing specific surface area. However, as described above, increasing surface area results in a decrease to volumetric capacity. Typically, improvements to surface area occur via creation of larger micro pores, thereby decreasing the crystal and bulk densities. Fig. 1 demonstrates this tradeoff by plotting the BET specific surface area ($S_A$) as a function of micropore volume ($V_{micro}$) for several MOFs in the literature (Data in Fig. 1 is taken from Refs. [10,49,50] and references therein). It is clear that there is a direct relationship between BET surface area and micropore volume with a correlation factor of 2160 $m^2$ BET surface area per $cm^3$ of pore volume which is consistent with previous literature for carbon aerogels [Literature value 2559 $m^2/cm^3$] [51]. Thus, it is important to identify approaches that enhance both gravimetric and volumetric density simultaneously. As is evident in Fig. 1, MOF-5 represents a good compromise between gravimetric and volumetric hydrogen capacity.

We calculated the $S_A$ and $V_{micro}$ for MOF-5 based on nitrogen and argon adsorption isotherms collected at 77 and 87 K, respectively. Experimental details for sample pretreatment and data collection can be found in Section 2.2.2 above. Based on these data, the $S_A$, $V_{micro}$, and mean pore width for MOF-5 are 2763 $m^2$ $g^{-1}$, 1.27 $cm^3$ $g^{-1}$, and 0.99 nm respectively. These $S_A$ and $V_{micro}$ data correlate well with literature values [32]. Additionally, the mean pore width value is close to that expected based on the fixed pore diameters measured from crystal structure data (1.1 and 1.5 nm).

#### 3.1.2. Crystallite and particle size

Particle and crystallite size can have implications for packing density in a packed bed hydrogen storage system. (Here we use "crystallite" to refer to a single crystal of MOF-5, and "particle" to refer to an agglomerate of crystallites.) Particle sizes of less than 100 m have been associated with increased interparticle friction; contributions from short-range electrostatic forces can also lead to agglomeration and inhibit packing [52]. Small particle size can also lead to an increased contribution of external surface area and intraparticle porosity, as well as decreased permeability and particle strength.

Scanning electron microscopy (SEM) was used to characterize the crystallite size for as-synthesized MOF-5 powder. A representative SEM image is shown in Fig. 2 (inset), where a cubic morphology is observed. The crystallite size histogram comprising data from three separate SEM images is also shown in Fig. 2. Based on a total of 182 crystallites, the mean crystallite size is

**Table 2**
Summary of structural, thermal, and hydrogen isotherm materials properties for MOF-5. Unless otherwise indicated, all measurements performed on loose powder form of MOF-5. Hydrogen isotherm parameters are based on fitting to 77, 138, 200, and 295 K isotherms from 0 to 100 bar.

| | Units | Value | Conditions |
|---|---|---|---|
| *Structure properties* | | | |
| Bulk density ($\rho_{bulk}$) | g $cm^{-3}$ | 0.13 | Limited manual taps |
| | | 0.22 | Tapping w/jolting volumeter |
| Framework density ($\rho_{fm}$) | g $cm^{-3}$ | 2.03 | |
| BET specific surface area ($S_A$) | $m^2$ $g^{-1}$ | 2763 | $N_2$ isotherm 77 K |
| Micropore volume ($V_{micro}$) | $cm^3$ $g^{-1}$ | 1.27 | Ar isotherm 87 K |
| Mean particle diameter | μm | 0.36 | |
| *Thermal properties* | | | |
| Thermal conductivity ($k$) | W $m^{-1}K^{-1}$ | 0.091 | 300 K, $\rho$ = 0.35 g $cm^{-3}$ |
| Heat capacity ($c_p$) | J $g^{-1}K^{-1}$ | 0.72 | 300 K |
| *Hydrogen isotherm parameters* | | | |
| $\alpha$ | J $mol^{-1}$ | 2239 | |
| $\beta$ | J $mol^{-1}K^{-1}$ | 19.5 | |
| $n_{max}$ | mol $kg^{-1}$ | 125.4 | |
| $P_o$ | MPa | 1692 | |
| $V_a$ | ml $g^{-1}$ | 2.01 | |

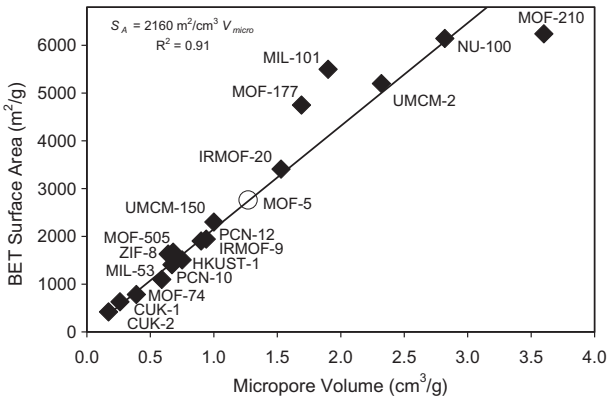


**Fig. 1.** Relationship between micropore volume ($V_{micro}$) and BET specific surface area ($S_A$) for several metal–organic frameworks. Values for $V_{micro}$ and $S_A$ adapted from Ref. [10] and references therein, and from Refs. [49,50].

0.36 ± 0.011 μm. As described below, this small crystal size of MOF-5 results in a relatively small bulk density (21% of the single crystalline value) as compared to other MOFs possessing larger crystal sizes.

In addition to measuring the crystallite size, the dimensions of agglomerated particles were also measured. The distribution of particle sizes and the cumulative percentage of their volume fraction is shown in Fig. 3. The mean of the particle size was found to be 0.22 mm, and 99% of the particles were found to have a diameter less than 0.86 mm. Comparison of the crystallite and particle size distributions indicates that due to inter-particle cohesion, essentially all sub-micron sized MOF-5 crystallites aggregate into particles having diameters larger than ~3 micron.

### 3.1.3. Bulk density

The bulk density of MOF-5 powder was initially measured using a small container (.75 mL) which was filled with MOF-5 and then tapped for approximately 5 s. This procedure resulted in a low density of 0.13 g/cm$^3$. To assess the effect of tapping upon bulk density, we loaded a known mass of MOF-5 powder into a larger graduated cylinder (25 cm$^3$), and manually tapped the cylinder on the floor of the glovebox; the cylinder elevation for each tap was 2–3 cm. The tapping process was repeated for an increasing number of taps, and the volume and mass of MOF-5 powder in the cylinder was recorded afterwards.

Fig. 4 shows the bulk density as a function of the number of manual taps. It is clear that the powder density increases with

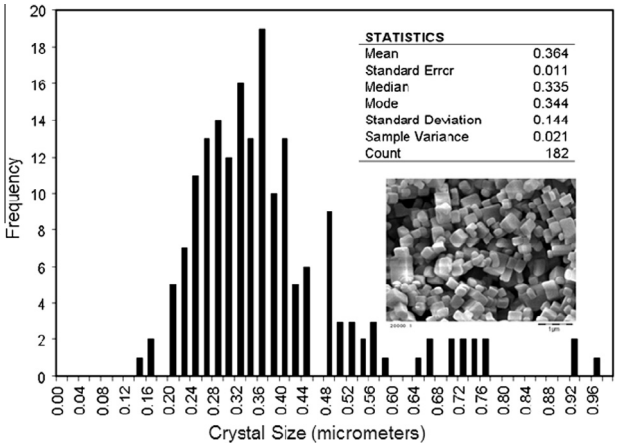


**Fig. 2.** Crystal size histogram and statistics for MOF-5 powder. The distribution has a mean diameter of 0.36 μm and standard deviation of 0.144 μm.

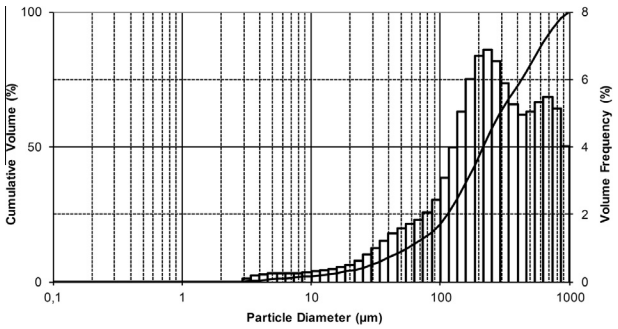


**Fig. 3.** Particle size distribution and cumulative volume percentage for a representative MOF-5 powder. The distribution has a mean diameter of 215 μm; 99% of the particles have a diameter less than 857 μm.

the number of taps, starting from a value of 0.18 g/cm$^3$ at 200 manual taps and increasing to 0.21 g/cm$^3$ after 2000 taps. The MOF-5 tap density was also measured using a standardized jolting volumeter. In this case a series of 2000 taps were used, and the resulting density of 0.22 g/cm$^3$ was found to be in very good agreement with the manually-tapped sample. Additional testing demonstrated that the tap density can depend on the volume of the graduated cylinder employed and on the particle size. These tests resulted in a range of MOF-5 powder densities spanning 0.13–0.22 g/cm$^3$.

### 3.2. Thermal properties

Although significant attention has been focused on improving the gas storage capacity of MOFs, relatively little effort has been devoted to assessing their thermal properties [53]. The thermal conductivity and heat capacity of MOFs (and other adsorbents) are significant because they will impact the design, performance, and cost of MOF-based storage systems [54–56]. For example, hydrogen uptake and release reactions involve the liberation (adsorption) or consumption (desorption) of heat; therefore efficient dissipation and delivery of heat is critical. Typically, adsorbent systems incorporate a heat exchanger for managing the temperature during fueling and delivery. The thermal conductivity properties of the storage media will have a direct influence on the heat exchanger design. If the thermal conductivity is low, the heat exchanger design requires additional complexity, which may add weight and cost. As a counter-measure, material enhancements (e.g. graphite additions) can be added to the material to increase the thermal conductivity. These additions displace some fraction of the storage material, resulting in a decrease in storage capacity and an increase in the system weight. Therefore, it is important to accurately evaluate thermal conductivity to minimize the amount of the enhancement materials. Moreover, the creation of accurate

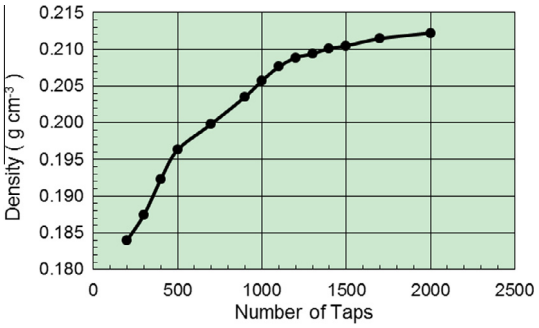


**Fig. 4.** Tap density of MOF-5 as a function of the number of taps.

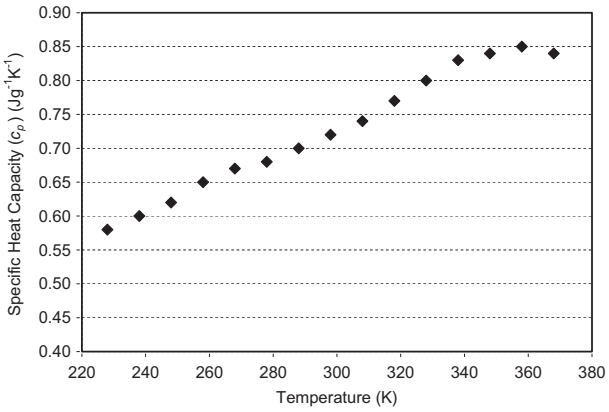


**Fig. 5.** Specific heat capacity ($c_p$) (J g$^{-1}$ K$^{-1}$) for powder MOF-5 as a function of temperature (K).

system models relies on the determination of thermal properties for materials of interest.

### 3.2.1. Heat capacity

The specific heat capacity ($c_p$) describes to the ability of a material to store thermal energy, and indicates the amount of energy needed to heat the material to a specified temperature. It is an important property for systems whose operation involves a temperature swing, such as in the thermal desorption of stored gasses. The heat capacity of powder MOF-5 in the temperature range of 220–370 K was determined using the procedure described in Section 2.2.5, and is plotted in Fig. 5. At 300 K, $c_p$ for MOF-5 was measured to be 0.72 J g$^{-1}$ K$^{-1}$, which is comparable to that of alumina (0.77 J g$^{-1}$ K$^{-1}$) and graphite (0.71 J g$^{-1}$ K$^{-1}$). $c_p$ increases approximately 33% over the measured temperature range, from approximately 0.6 J g$^{-1}$ K$^{-1}$ at 220 K to 0.8 J g$^{-1}$ K$^{-1}$ at 340 K.

### 3.2.2. Thermal conductivity

The thermal conductivity of most microporous materials (e.g. zeolites and MOFs) is low, stemming from their large pore size (>20 Å in diameter) and high free volume (>90% free volume). McCaughey et al. have pointed out that the atomic number density for MOFs is even lower than that for zeolites ($2.46 \times 10^{28}$ atoms/m$^3$ for MOF-5 verses $5.13 \times 10^{28}$ atoms/m$^3$ for sodalite), suggesting that MOFs will have an even lower thermal conductivity than other highly porous compounds [57]. Single crystal thermal conductivity measurements have been previously measured on 1–2 mm crystals of MOF-5 over a temperature range of 6–300 K in Ref. [58]. This data, obtained using a longitudinal steady-state heat flow method, shows a peak thermal conductivity at 20 K of ~0.37 W/m K and a minimum at 100 K of ~0.22 W/m K. From 100 to 300 K, the thermal conductivity increases by 30%, attaining a value at 300 K of ~0.32 W/m K. This value is much lower than that for other microporous single crystals such as zeolites (3.53 and 2.07 W/m K for sodalite and faujasite, respectively) [53].

The intrinsic thermal conductivity for MOF-5 single-crystals represents an upper limit for the pure material. Data from powder samples includes the effects of interparticle porosity which will reduce the thermal conductivity below the single crystal value. We have measured the thermal conductivity for compacted MOF-5 powder at temperatures from 300 to 335 K and at three densities: 0.35, 0.52, and 0.69 g/cm$^3$. The thermal conductivity ($k$) was calculated as the product of heat capacity ($c_p$) [see Section 3.2.1, thermal diffusivity ($\alpha$) and bulk density ($\rho$). See Section 2.2.4 to Section 2.2.6 for experimental details. Measured thermal conductivity data is plotted in Fig. 6. The thermal conductivity for MOF-5 remains relatively constant over the measured temperature range for all three densities. Values at 300 K for each density are as follows: 0.091 W m$^{-1}$ K$^{-1}$ ($\rho$ = 0.35 g cm$^{-3}$), 0.11 W m$^{-1}$ K$^{-1}$ ($\rho$ = 0.52 g cm$^{-3}$), and 0.16 W m$^{-1}$ K$^{-1}$ ($\rho$ = 0.69 g cm$^{-3}$). (As the highest density pellets exceed the single-crystal density we presume some plastic deformation such as pore collapse has occurred in these samples during the compression process.) Based on these data, a modest improvement in $k$ can be achieved via compression of the neat powder (e.g. ~20% improvement in $k$ in going from $\rho$ = 0.35–0.52 g cm$^{-3}$). The thermal conductivity for the 0.52 g cm$^{-3}$ compact at 300 K is only 35% of the value of that for the single crystal ($\rho$ = 0.61 g cm$^{-3}$) and is comparable to that of other hydrogen storage materials such as sodium alanate (~0.5 W m$^{-1}$ K$^{-1}$) [59]. Since higher thermal conductivities are desirable, the addition of conductive additives such as graphite or aluminum (e.g. graphite has a thermal conductivity of 1390 Wm$^{-1}$K$^{-1}$ at 400 K)[60] will likely be required to improve heat transfer. The impact of expanded natural graphite additives (ENG) on thermal conductivity of MOF-5/ENG compacts has been studied recently [51].

## 3.3. Hydrogen adsorption isotherms

Hydrogen isotherm data is essential for constructing system models for capacity and dormancy under various operating scenarios. Toward this end, materials-level models that can describe empirical hydrogen adsorption isotherm data are needed. Until recently, efforts aimed at identifying such models have been scarce due to the complexities of performing measurements at multiple sub-ambient temperatures. For example, most measurements on sorbents have been limited to a small number of temperatures that are accessible using cryogenic baths (e.g. liquid nitrogen, liquid argon, solid $CO_2$). In this work, a continuous flow controlled cryostat is employed for collection of adsorption data at several intermediate temperatures: 103, 118, and 138 K. Cryogenic baths are used for 77 and 200 K, while measurements at 295 K are performed without active temperature control. The resulting data is then used to determine model parameters that in turn provide an analytic expression for the adsorption properties in MOF-5 at arbitrary temperatures.

### 3.3.1. Modeling approach

Hydrogen adsorption data can be expressed in various forms, for example excess, absolute, or total adsorbed amounts [33]. The excess amount adsorbed ($n_{ex}$) is defined as the amount of adsor-

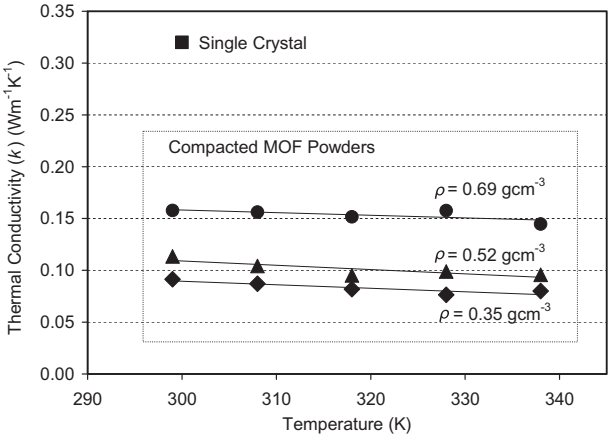


**Fig. 6.** Thermal conductivity data for MOF-5 powders as a function of temperature and bulk density: 0.35 g cm$^{-3}$ (diamonds), 0.52 g cm$^{-3}$ (triangles) and 0.69 g cm$^{-3}$ (circles). The thermal conductivity for a single crystal of MOF-5 at 300 K (square) is provided for Ref. [58].

bate (e.g., hydrogen) stored in the porous volume of an adsorbent (e.g., MOF) at a given temperature and pressure above and beyond what would be present in the same volume in the absence of adsorbate-adsorbent interactions. The absolute amount adsorbed ($n_a$) is defined as the quantity of adsorbate molecules in the adsorption volume ($V_a$), including specifically adsorbed molecules as well as gas phase molecules. Finally, the total amount ($n_{tot.}$) represents the total amount of hydrogen stored in the hydrogen storage system and includes contributions of $n_a$ and homogeneous bulk hydrogen gas ($n_g$) which can occupy interparticle and intraparticle voids. While excess isotherms are typically determined experimentally, absolute adsorption data is often an estimated value. Excess and absolute adsorption data are related by Eq. (1) [61].

$$n_{ex} = n_a - \rho_g V_a \tag{1}$$

where $\rho_g$ denotes the density of bulk gas, and the volume occupied by the adsorbed phase, $V_a$, is assumed to be a constant. During adsorption the adsorbed gas occupies the space $V_a$ spanned by the adsorption field generated by the adsorbent, and the average adsorbate density gradually increases up to an asymptotic value [33]. From Eq. (1), we can also infer that near ambient conditions (e.g., low pressure and/or above cryogenic temperatures), $\rho_g$ will be significantly lower than the density of the adsorbed phase ($\rho_a$). Under such conditions, the approximation $n_e x \equiv n_a$ holds. However, at higher pressures and/or cryogenic temperatures the density of the gas phase ($\rho_g$) increases at a faster rate than the density of the absorbed phase ($\rho_a$), and thus $n_a$ will continue to increase as $n_{ex}$ reaches a maximum (plateau).

The Dubinin–Astakhov (D–A) model [21] is a pore filling model for adsorption of subcritical gases in microporous adsorbents, i.e., those whose pore diameter is less than 2 nm. This model has been adapted to describe supercritical $H_2$ adsorption for a variety of microporous materials (e.g. carbons and MOFs). For these compounds the adsorption enthalpy is influenced by the superposition of attractive forces from neighboring walls of the adsorbent. In such microporous materials, the adsorption process is often interpreted as a volume of liquid adsorbate filling the pores. The D–A model can be readily applied to most MOFs given that their pore diameters (0.5–1.5 nm) fall within the applicable range. (The diameters of the two pores in MOF-5 are 1.5 and 1.1 nm.) Herein, we employ a modification of the D–A model [62] where excess adsorption is defined as:

$$n_{\mathrm{ex}} = n_{\max} \exp\left[-\left[\frac{\mathrm{RT}}{\alpha + \beta T}\right]^m \ln^m\left(\frac{P_0}{P}\right)\right] - \rho_g V_a \tag{2}$$

where $\alpha$ and $\beta$ are enthalpic and entropic contributions to the characteristic free energy of adsorption, $m$ is the heterogeneity parameter, and $P_0$, is the pressure corresponding to the limiting adsorption. One feature of Eq. (2) is the temperature-dependent expression of the characteristic free energy of adsorption ($\in$), where $\epsilon = \alpha + \beta T$. Other approaches, including modifications of the D–A model and monolayer-based models (Unilan and Toth), have recently been used to fit MOF-5 hydrogen adsorption isotherms [22,63].

### 3.3.2. Experimental and modeling results for excess capacity

The excess hydrogen adsorption ($n_{ex}$) by MOF-5 as a function of temperature (77–295 K) and pressure (0–100 bar) is shown in Fig. 7. The storage capacities are expressed as excess gravimetric capacity (expressed as wt.%) and excess volumetric capacity (g $H_2$/L·MOF-5). The experimental data are represented by symbols and the modeled fits by the solid lines. The measured excess adsorption at 77 K shows a maximum value of 6.0 wt.% (29.9 mol/kg) at 48 bar. (In the present study wt.% is defined as (g $H_2$/g MOF-5) × 100.) This value is comparable to previous measurements for MOF-5 powder, which vary between 4.7 and 7.1 wt.% [2]. As is expected, the adsorption decreases with increasing temperature. For example, at a temperature of 200 K and 80 bar, the maximum gravimetric capacity is only 1.3 wt.% (6.4 mol/kg).

The excess volumetric adsorption at its maximum value, based on the density for loosely-packed powder MOF-5 ($\rho_{pwd}$ = 0.13 - g cm$^{-3}$), is approximately 8 g $H_2$/L·MOF-5 (near-right ordinate, Fig. 7) as compared to 36 g $H_2$/L (rightmost ordinate, Fig. 7) assuming a single crystal density ($\rho_{sx}$ = 0.605 g cm$^{-3}$). The powder and single-crystal morphologies represent the extremes of volumetric capacity in MOF-5. In principle, intermediate capacities may be achieved via materials engineering. For example, in a prior study we examined the extent to which volumetric density could be improved in MOF-5 via densification [22,23].

Parametric description of the excess hydrogen stored in MOF-5 as a function of temperature and pressure was achieved by fitting the modified D-A model (Eq. (2)) with $m$ = 2. Values for the five parameters, $n_{max}$, $\alpha$, $\beta$, $P_0$, and $V_a$, were obtained by nonlinear regression on the measured isotherms at 77, 138, 200 and 295 K. The resulting values for the model parameters are listed in Table 2, and the fits are represented as solid lines in Fig. 7. Here, the value for the adsorbed volume ($V_a$) is 2.01 cm$^3$ g$^{-1}$. The remaining parameter values, $n_{max}$ = 125.4 mol/kg, $\alpha$ = 2239 J mol$^{-1}$, $\beta$ = 19.5 J mol$^{-1}$ K$^{-1}$, and $P_0$ = 1692 MPa, are of comparable magnitude to those previously established [62] for AX-21.

As can be seen in Fig. 7, the D–A model parameters for MOF-5 reproduce the empirical data across the measured temperature–pressure conditions (e.g. 77–298 K and 0–100 bar). Nevertheless the original intent of the various adsorption models was to impart physical insight into the adsorption process (e.g., $\alpha$ represents the enthalpic contribution to the free energy of adsorption). Given the empirical nature of the model, its various modifications, and its applicability to the MOF materials class, the clear physical meaning of the parameters becomes more ambiguous. In particular, we find the estimated adsorption volume ($V_a$ = 2.01 ml/g) is larger than the intra-crystalline pore volume, given by $1/\rho_{\mathrm{sx}} - 1/\rho_{\mathrm{fm}}$ = 1.16 ml/g, as well as the experimentally determined micropore volume ($V_{micro}$) of 1.2 ml/g [as reported in Section 3.1.1]. Likewise, the parameters ($n_{\max}$ in particular) obtained here by fits to data between 77 and 295 K over-predict the expected excess adsorption at 30 K by at least 20% [64]. We also note that the modeled excess adsorption at 295 K is negative below a pressure of approximately 20 bar. Thus caution should be exercised in applying these parameterizations to operating conditions outside of the ones used here.

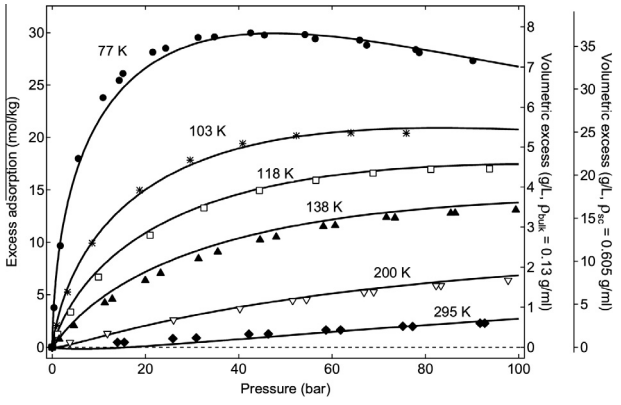


**Fig. 7.** Excess hydrogen adsorption isotherms for powder MOF-5 at five temperatures (77, 103, 118, 138, 200 and 295 K). Measured data corresponds to symbol points, and solid lines are fits using the modified D–A Eq. (2). (Left axis) Gravimetric excess capacity in mol/kg. (Right axes) Volumetric excess adsorption (g/L), where the near-right ordinate is based on the MOF-5 loose-packed powder density ($\rho_{bulk}$ = 0.13 g cm$^{-3}$) and the rightmost ordinate assumes a density equal to the MOF-5 crystal density ($\rho_{sx}$ = 0.605 g cm$^{-3}$).

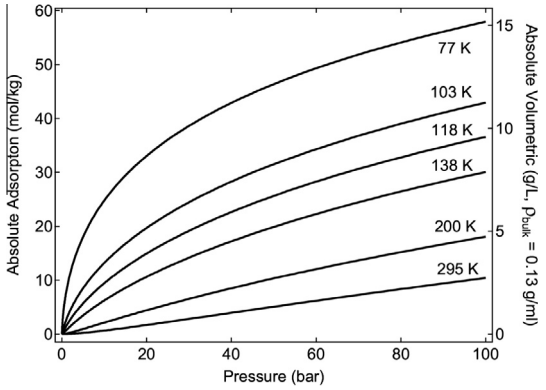


**Fig. 8.** Absolute hydrogen adsorption isotherms for powder MOF-5 at six temperatures (77, 103, 118, 138, 200, and 295 K) based on D–A parameters in Section 3.3.2. On the left ordinate, absolute adsorption is listed in gravimetric units of mol/kg. The right ordinate lists absolute adsorption in volumetric units of g/L, assuming the bulk density of loosely-packed MOF-5 powder ($\rho_{bulk}$ = 0.13 g cm$^{-3}$).

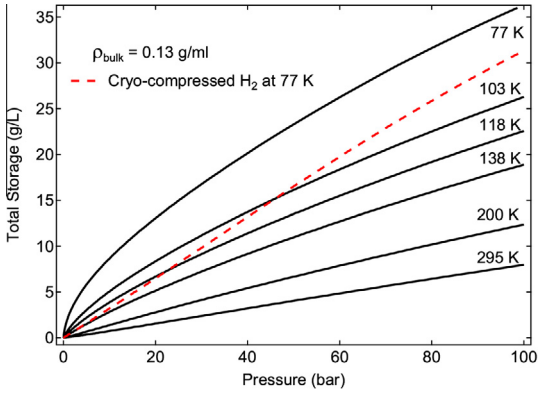


**Fig. 9.** Total hydrogen storage within the gross volume occupied by the powder MOF-5, assuming a bulk powder density of $\rho_{bulk}$ = 0.13 g/cm$^3$. The dashed red line indicates the density of bulk $H_2$ gas at 77 K. (For interpretation of the references to color in this figure legend, the reader is referred to the web version of this article.)

Other models, including the Unilan model, have been found to better describe $H_2$ adsorption by MOF-5 over a wide range of temperature [22].

### 3.3.3. Modeled absolute and total capacity

MOF-5 absolute hydrogen isotherms based on the modified D-A model are shown in Fig. 8. The absolute capacity includes excess adsorption as well as gas that is contained within the adsorption volume, $V_a$, according to Eq. (1) above. At low temperatures and high pressures, the amount of additional gas in the adsorption volume is appreciable. Consequently, the absolute adsorption amount can be nearly double that of the excess gravimetric capacity. For example, at 77 K and 75 bar, $n_{ex}$ and $n_a$ for MOF-5 are 5.8 and 10.7 wt.% respectively. Absolute $H_2$ uptake on a volumetric basis for bulk MOF-5 powder is provided on the right ordinate in Fig. 8

For practical applications the total amount of stored hydrogen, $n_{tot}$, where $n_{tot} = n_{ex} + \rho_g V_v$ and $V_v = 1/\rho_{bulk} - 1/\rho_{sk}$ is of the most importance. The total capacity MOF-5 depends on the temperature and pressure of operation (which affect $\rho_g$) and on the bulk adsorbent density (which affects the void volume, $V_v$). The total volumetric storage, estimated by multiplying the gravimetric total storage, $n_{tot}$, by the bulk density, $\rho_{bulk}$, is shown Fig 9. The MOF-5 powder density (0.13 g cm$^{-3}$, loose-packed) is used as the bulk density. Total volumetric capacities are compared with that of compressed $H_2$ at 77 K, which is illustrated as a dashed line in Fig. 9. It can be seen that MOF-5 powder, even in a loosely-packed form, increases the $H_2$ storage capacity for temperatures below 200 K. This enhancement in volumetric storage capacity is considerably larger if one considers a MOF-5 single crystal (assuming the gravimetric capacity is the same for both MOF-5 powder and monoliths). The "breakeven" pressure is the point at which the total storage of compressed $H_2$ exceeds that of the sorbent, at which point the sorbent provides no net benefit. At 77 K, the breakeven point (~386 bar) that is estimated from the D–A parameters in Table 2 occurs outside of the experimental 0–100 bar pressure range.

### 3.3.4. Adsorption enthalpy

The differential enthalpy of adsorption ($\Delta H_{ads}$) for sorbents such as MOF-5 is an important parameter that, together with thermal attributes discussed above, affects the overall design and performance of on-board and/or forecourt thermal management systems. The amount of heat to be liberated from the storage bed during adsorption is related to the $\Delta H_{ads}$. Here, we have calculated $\Delta H_{ads}$ as a function of excess hydrogen adsorption in MOF-5 by applying the Clausius–Clapeyron equation to excess adsorption isotherms. An estimate of $\Delta H_{ads}$ from experimental isotherms is plotted versus fractional excess adsorption (i.e., $n_{ex}$ divided by $n_{max}$ from Table 2) in Fig. 10. The magnitude of the enthalpy decreases from about −5 kJ/mol at zero coverage to −4.3 kJ/mol at a fractional excess uptake of about 0.1, consistent with results previously published for powder MOF-5 [22]

The differential enthalpy of adsorption can also be calculated analytically for the modified D–A model as a function of absolute adsorption: [65]

$$\Delta H_{ads} = -\alpha\sqrt{-\ln(n_a/n_{max})} \quad (3)$$

Eq. (3) is plotted in Fig. 10 using the D–A parameters listed in Table 2. At low pressures, the excess and absolute adsorption amounts are similar, and thus the experimental and modeled $\Delta H_{ads}$ can be directly compared. Agreement between the experimental and modeled enthalpy is very good. These results confirm that adsorption models such (as the D–A model) are effective in describing the equilibrium PCT diagrams of $H_2$/MOF-5, and in modeling the thermodynamic properties of cryo-adsorption-based hydrogen storage. Further, these D–A parameter values can be used in the governing equations for heat and mass conservation in a hydrogen storage model for MOF-5.

### 3.4. Robustness to air exposure

The robustness of MOFs with respect to air and/or water has attracted considerable attention during the past few years

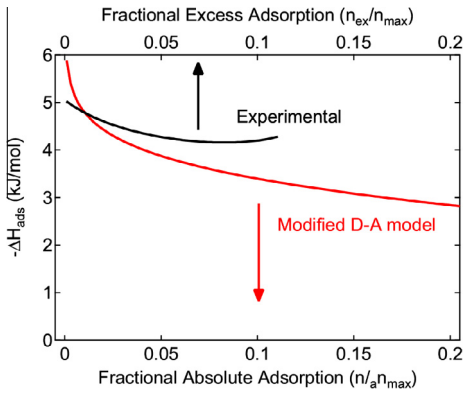


**Fig. 10.** Differential $H_2$ adsorption enthalpy ($-\Delta H_{ads}$) of powder MOF-5. Experimental estimates of $-\Delta H_{ads}$ are plotted on the top axis versus the fractional excess adsorption. The modeled $-\Delta H_{ads}$ (Eq. 5) is plotted on the bottom axis versus fractional absolute adsorption.

[48,66–72], with many authors observing some degree of degradation following exposure. Given that stability is a desirable property – for example, assembly of a MOF-based gas storage system would be less costly if it could be performed in open air – here we examine the robustness of the pilot-scale version of MOF-5. Changes to the hydrogen adsorption properties and crystal structure of MOF-5 powders as a function of exposure time to humid air (45% relative humidity at 22 °C) are summarized in Figs. 11 and 12, respectively. Overall, the data suggests only a minor degradation of properties for exposure times up to 8 h. Regarding the impact on hydrogen uptake, Fig. 11 compares the effects of exposure time and sample activation on excess $H_2$ adsorption. (A magnification of the maximum uptake region is shown as an inset.) For the shortest exposure time of 12 min a 1.2–1.5% decrease in maximum uptake from the baseline, (i.e., non-exposed) sample is observed for the activated and non-activated samples, respectively. At 1.5 h of exposure the reduction in uptake increases only slightly (3.5–3.7%, activated vs. non-activated). Finally, for the longest exposure time of 8 h the reduction in excess $H_2$ adsorption is 7.3%. Since it is unlikely that activation could reverse ligand displacement or loss of crystallinity, the similarity in uptake for the activated vs. non-activated samples suggests that the degree of irreversible structure change occurring in MOF-5 under these conditions is relatively small.

To confirm the $H_2$ uptake measurements, Fig. 12 plots *in situ* X-ray diffraction patterns for samples continuously exposed to humid, laboratory air for times up to 250 h. With increasing exposure time we observe a reduction in intensity for the diffraction peak at 7°. A new peak at 9° appears only after the sample is exposed for more than 100 h. The emergence of this peak is similar to what has been observed in previous work [48] after 10 min exposure time. Unfortunately, the humidity conditions used in Ref. [48] were not reported; therefore a direct comparison is not straightforward. Nevertheless, such a difference could be traced to one or more factors, such as differences in MOF composition, initial structure, sample mass, and/or exposure conditions (humidity levels, exposure time, temperature, static/flowing exposure, etc.) For example, we observe some initial differences in the low-angle diffraction peaks in our samples compared to other literature reports [48,66,70–72], which could indicate the presence of retained salt or solvent.

We conclude that the robustness of the MOF-5 powder suggested by our PCT data is consistent with the XRD patterns. Taken together, these data suggest that brief exposure of MOF-5 (for example, during the few minutes needed to load/assemble a pressure vessel) should not result in significant reductions in performance. Additional studies are planned to more quantitatively assess the impact of factors such as higher humidity levels and compaction [22,23].

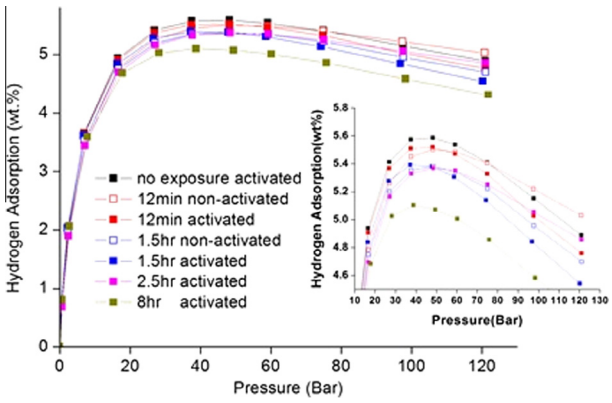


**Fig. 11.** MOF-5 hydrogen uptake isotherms following exposure to humid air (45% relative humidity at 22 °C) for various times. "Activated" samples were heated to 130 °C and evacuated for at least 6 h; "non-activated" samples were evacuated without heating for only 15 min. The inset shows a magnification of the maximum uptake region of the isotherms.

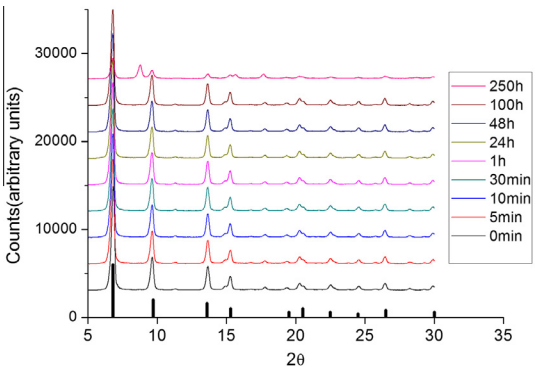


**Fig. 12.** *In situ* X-ray diffraction pattern for MOF-5 powder as a function of exposure time to laboratory air (relative humidity around 45% at 22 °C). Vertical lines show the peak positions and relative intensities for the reference desolvated MOF-5 structure [24].

## 4. Conclusions

We have performed a comprehensive assessment of the primary thermo-physical properties of MOF-5 powders. Characterized properties include: packing density, surface area, pore volume, particle size distribution, thermal conductivity, heat capacity, stability against hydrolysis, differential enthalpy of $H_2$ adsorption, and Dubinin–Astakhov isotherm parameters. Although some of the characterized properties have been previously reported for laboratory-scale (i.e., small) quantities of MOF-5, variation arising from differences in MOF synthesis and activation pose challenges to achieving a consistent description of these properties. The present study aims to minimize these inconsistencies by analyzing an industrial, pilot-scale version of MOF-5. Consequently, the data should provide a reasonable approximation to the properties expected in industrial applications. Although here we emphasize properties relevant for hydrogen storage, the data can serve as a starting point for MOF-based systems in other applications such as catalysis, gas separations, etc.

The pilot-scale synthesis method described here using zinc acetate dihydrate yields a robust MOF-5 powder with good resistance to humidity degradation: Exposure to air (45% relative humidity, 22 °C) for 1.5 h resulted in only a ~3.5% reduction in excess $H_2$ uptake. The mean crystal diameter of the resulting finely-powdered MOF-5 was measured at 0.36 μm. The packing density of the powder is sensitive to the degree of tapping, and can vary from 0.13 to 0.22 g $cm^{-3}$. The powder can be easily shaped into pellets by uniaxial compaction, without the need for binder. Porous texture measurements indicate a BET specific surface area of 2763 $m^2$ $g^{-1}$ and a micropore volume of 1.27 $cm^3$ $g^{-1}$. The thermal conductivity of 0.35 g $cm^{-3}$ MOF-5 pellets was measured to be 0.091 W $m^{-1}K^{-1}$ at 300 K. The heat capacity, $c_p$, of powder MOF-5 in the temperature range of 220–370 K was determined; at 300 K, $c_p = 0.72$ $Jg^{-1}K^{-1}$. We determined parameters for the modified Dubinin–Astakhov isotherm model, which accurately describes the concentration of adsorbed $H_2$ within MOF-5 over the temperature range 77–295 K and the pressure range 0–100 bar.

## Acknowledgement

Financial support for this study was provided by the US Department of Energy, Office of Energy Efficiency and Renewable Energy, Grant no. DE-FC36-GO19002.

## References


[1] J.L.C. Rowsell, O.M. Yaghi, Microporous Mesoporous Mater. 73 (2004) 3–14.
[2] M.P. Suh, H.J. Park, T.K. Prasad, D. Lim, Chem. Rev. 112 (2012) 782–835.
[3] S.T. Meek, J.A. Greathouse, M.D. Allendorf, Adv. Mater. 23 (2011) 249–267.
[4] A.U. Czaja, N. Trukhan, U. Müller, Chem. Soc. Rev. 38 (2009) 1284–1293.
[5] C. Wang, D. Liu, W. Lin, J. Am. Chem. Soc. 36 (2013) 13222–13234.
[6] J.Y. Jung, F. Karadas, S. Zulfiqar, E. Deniz, S. Aparicio, M. Atilhan, C.T. Yavuz, S.M. Han, Phys. Chem. Chem. Phys. 15 (2013) 14319.
[7] Y. Yu, Y. Ren, W. Shen, H. Deng, Z. Gao, Trends Anal. Chem. 50 (2013) 33–41.
[8] M. Sindoro, A. Jee, S. Granick, Chem. Commun. 49 (2013) 9576–9578.
[9] N.T.S. Phan, P.H.L. Vu, T.T. Nguyen, J. Catal. 306 (2013) 38–46.
[10] L.J. Murray, M. Dinca, J.R. Long, Chem. Soc. Rev. 38 (2009) 1294–1314.
[11] J.L.C. Rowsell, O.M. Yaghi, Angew. Chem., Int. Ed. 44 (2005) 4670–4679.
[12] R.K. Ahluwalia, J.K. Peng, Int. J. Hydrogen Energy 34 (2009) 5476–5487.
[13] M. Lamari, A. Aoufi, P. Malbrunot, AIChE J. 46 (2000) 632–646.
[14] L. Huang, H. Wang, J. Chen, Z. Wang, J. Sun, D. Zhao, Y. Yan, Microporous Mesoporous Mater. 58 (2003) 105–114.
[15] J.L.C. Roswell, A.R. Millward, K.S. Park, O.M. Yaghi, J. Am. Chem. Soc. 126 (2004) 5666–5667.
[16] M. Eddaoudi, D.B. Moler, H. Li, B. Chen, T.M. Reineke, M. O'Keeffe, O.M. Yaghi, Acc. Chem. Res. 34 (2001) 319–330.
[17] B. Panella, M. Hirscher, Adv. Mater. 17 (2005) 538–541.
[18] M. Jacoby, Chem. Engg. News (2008) 13–16.
[19] M. Gaab, N. Trukhan, S. Maurer, R. Gummaraju, U. Müller, Microporous Mesoporous Mater. 157 (2012) 131–136.
[20] H. Li, M. Eddaoudi, M. O'keeffe, O.M. Yaghi, Nature 402 (1999) 276–279.
[21] M. Dubinin, V. Astakhov, Adv. Chem. Ser. 102 (1971) 69–85.
[22] J. Purewal, D. Liu, A. Sudik, M. Veenstra, J. Yang, S. Maurer, J. Phys. Chem. C 116 (2012) 20199–20212.
[23] J.J. Purewal, D. Liu, J. Yang, A. Sudik, D.J. Siegel, S. Maurer, U. Muller, Int. J. Hydrogen Energy 37 (2012) 2723–2727.
[24] D.J. Tranchemontagne, J.R. Hunt, O.M. Yaghi, Tetrahedron 64 (2008) 8553–8557.
[25] A.P. Nelson, O.K. Farha, K.L. Mulfort, J.T. Hupp, J. Am. Chem. Soc. 131 (2009) 458–460.
[26] S. Brunauer, P.H. Emmett, E. Teller, J. Am. Chem. Soc. 60 (1938) 309–319.
[27] E.P. Barrett, L.G. Joyner, P.P. Halenda, J. Am. Chem. Soc. 73 (1951) 373–380.
[28] W.S. Rasband, ImageJ, U.S. National Institutes of Health, Bethesda, Maryland, USA. http://rsb.info.nih.gov/ij/, 1997–2005.
[29] R. Zacharia, D. Cossement, L. Lafi, R. Chahine, J. Mater. Chem. 20 (2010) 2145–2151.
[30] A. Dailly, E. Poirier, Energy Environ. Sci. 4 (2011) 3527–3534.
[31] M. Jorda-Beneyto, D. Lozano-Castello, F. Suarez-Garcia, D. Cazorla-Amoros, A. Linares-Solano, Microporous Mesoporous Mater. 112 (2008) 235–242.
[32] D. Liu, J.J. Purewal, J. Yang, A. Sudik, S. Maurer, U. Müller, J. Ni, D.J. Siegel, Int. J. Hydrogen Energy 37 (2012) 6109–6117.
[33] K.J. Gross, K.R. Carrington, S. Barcelo, A. Karkamkar, J. Purewal, S. Ma, H. Zhou, P. Dantzer, K. Ott, T. Burrell, T. Semeslberger, Y. Pivak, B. Dam, D.Chandra, Recommended Best Practices for the Characterization of Storage Properties of Hydrogen Storage Materials, V3.34 (Feb 21, 2012). Available at: http://www1.eere.energy.gov/hydrogenandfuelcells/pdfs/best_practices_hydrogen_storage.pdf.
[34] J.W. Leachman, R.T. Jacobsen, S.G. Penoncello, E.W. Lemmon, J. Phys. Chem. 38 (2009) 721–748.
[35] E.W. Lemmon, M.L. Huber, M.O. McLinden, NIST Standard Reference Database 23: Reference Fluid Thermodynamic and Transport Properties—REPROP, Version 9.0, 2010.
[36] S. Hausdorf, J. Wagler, R. Mossig, F.O.R.L. Mertens, J. Phys. Chem. A 112 (2008) 7567–7576.
[37] J.A. Greathouse, M.D. Allendorf, J. Am. Chem. Soc. 128 (2006) 10678–10679.
[38] B. Panella, M. Hirscher, S. Roth, Carbon 43 (2005) 2009–2214.
[39] H. Kabbour, T.F. Baumann, J.H. Satcher, A. Saulnier, C.C. Ahn, Chem. Mater. 18 (2006) 6085–6087.
[40] R. Chahine, T.K. Bose, Characterization and Optimization of Adsorbents for Hydrogen Storage, 11th WHEC, Pergamon Press, Oxford, UK, 1996.
[41] J.-F. Le Page, Manufacture, Use of Solid Catalysts. (1987) 75–123.
[42] J. Purwal, D. Liu, J. Yang, A. Sudik, D.J. Siegel, S. Maurer, U. Muller, Int. J. Hydrogen Energy 37 (2012) 2723–2727.
[43] S. Ma, Chem. Commun. 46 (2010) 44–53.
[44] A. Züttel, P. Sudan, P. Mauron, P. Wenger, Appl. Phys. A: Mater. Sci. Process. 78 (2004) 941–946.
[45] H. Kabbour, T.F. Baumann, J.H. Satcher Jr, A. Saulnier, C.C. Ahn, Chem. Mater. 18 (2006) 6085.
[46] B. Panella, M. Hirscher, H. Puetter, U. Müller, Adv. Funct. Mat. 16 (2006) 520–524.
[47] H. Frost, J. Phys. Chem. B. 110 (2006) 9565–9570.
[48] S.S. Kaye, A. Dailly, O.M. Yaghi, J.R. Long, J. Am. Chem. Soc. 129 (2007) 14176–14177.
[49] O.K. Farha, A.Ö. Yazaydin, I. Eryazici, C.D. Malliakas, B.G. Hauser, M.G. Kanatzidis, S.T. Nguyen, R.Q. Snurr, J.T. Hupp, Nat. Chem. 2 (2010) 944.
[50] H. Furukawa, N. Ko, Y.B. Go, N. Aratani, S.B. Choi, E. Choi, A.Ö. Yazaydin, R.Q. Snurr, M. O'Keeffe, J. Kim, O.M. Yaghi, Science 23 (2010) 424.
[51] C. Scherdel, G. Reichenauer, M. Wiener, Microporous Mesoporous Mater. 132 (2010) 572–575.
[52] R.M. German, Particle Packing Characteristics, Metal Powder Industries Federations, Princeton, NJ, 1989.
[53] A.J.H. McMaughey, M. Kaviany, Int. J. Heat Mass Transfer 47 (2004) 1799–1816.
[54] S. Kumar, M. Raju, V.S. Kumar, Int. J. Hydrogen Energy (2011) In Press, doi:http://dx.doi.org/10.1016/j.ijhydene.2011.04.182.
[55] J. Xiao, L. Tong, C. Deng, P. Bénard, R. Chahine, Int. J. Hydrogen Energy 35 (2010) 8106–8116.
[56] M.-A. André, D. Cossement, P.-A. Chandonia, R. Chahine, D. Mori, K. Hirose, Energy Eng. 55 (2009) 2985–2996.
[57] R.W.G. Wyckoff, Crystal Structures, 2 ed., John Wiley and Sons, Interscience, New York, 1963.
[58] B.L. Huang, Z. Ni, A. Millward, A.J.H. McGaughey, C. Uher, M. Kaviany, O.M. Yaghi, Int. J. Heat Mass Transfer 50 (2007) 405–411.
[59] D.E. Dedrick, M.P. Kanouff, B.C. Replogle, K.J. Gross, J. Alloys Compd. 389 (2005) 299–305.
[60] F.P. Incropera, D.P. DeWitt, Fundamentals of Heat and Mass Transfer, John Wiley & Sons, New York, 1996.
[61] K. Murata, J. Miyawaki, K. Kaneko, Carbon 40 (2002) 425–428.
[62] M.-A. Richard, P. Bénard, R. Chahine, Adsorption 15 (2009) 43–51.
[63] E. Poirier, A. Dailly, J. Phys. Chem. C 112 (2008) 13047–13052.
[64] W. Zhou, M.R. Hartman, T. Yildirim, J. Phys. Chem. C 111 (2007) 16131–16137.
[65] M.-A. Richard, P. Bénard, R. Chahine, Adsorption 15 (2009) 53–63.
[66] J.J. Low, A.I. Benin, P. Jakubczak, J.F. Abrahamian, S.A. Faheem, R.R. Willis, J. Am. Chem. Soc. 131 (2009) 15834–15842.
[67] M. Sabo, A. Henschel, H. Frode, E. Klemm, S. Kaskel, J. Mater. Chem. 17 (2007) 3827.
[68] L. Bellarosa, S. Calero, N. Lopez, Phys. Chem. Chem. Phys. 14 (2012) 7240–7245.
[69] M. De, ChemPhysChem 13 (2012) 3497–3503.
[70] K. Schrock, F. Schroder, M. Heyden, R.A. Fischer, M. Havenith, Phys. Chem. Chem. Phys. 10 (2008) 4732–4739.
[71] J. Hafizovic, M. Bjørgen, U. Olsbye, P.D.C. Dietzel, S. Bordiga, C. Prestipino, C. Lamberti, K.P. Lillerud, J. Am. Chem. Soc. 129 (2007) 3612–3620.
[72] L. Huang, H. Wang, J. Chen, Z. Wang, J. Sun, D. Zhao, Y. Yan, Microporous Mesoporous Mater. 58 (2003) 105–114.